

CASE STUDY

# Enabling 3D Multiplexing Spatial Omics Workflows in Neuroscience

By ZEISS Microscopy

13 JANUARY 2024, 20 MIN READ



AUTHOR  
**Kalliopi Arkoudi**  
Applications Development Engineer  
ZEISS Microscopy



AUTHOR  
**Maria Burdyniuk**  
Applications Specialist  
ZEISS Microscopy



AUTHOR  
**Samantha Fore**  
Product Marketing Manager  
ZEISS Microscopy



AUTHOR  
**Birgitt Schuele**  
Associate Professor  
Stanford University



AUTHOR  
**Alejandra Morato Torres**  
Life science Research Professional  
Stanford University

# Enabling 3D Multiplexing Spatial Omics Workflows in Neuroscience

The series "From Image to Results" explores various case studies which present how to achieve quantifiable results from your imaging data. Each case study explores different samples, imaging systems, and research questions.

This case study provides a blueprint for the analysis of 3D spatial omics multiplexing datasets from a CODEX multiplex antibody panel imaged with a custom set-up using the Akoya Phenocycler and ZEISS LSM 980 confocal microscope to explore the expression of an extensive list of pre-synaptic markers in the mouse brain. A detailed description of 3D registration of spectral multiplexing data, AI object segmentation, and statistical analyses, including cell neighborhood and dimensionality reduction analyses, are provided. These can provide unique insights not only into neuroscience but also cancer research, immunology, and single-cell analysis experiments.

Key Learnings:

- 3D registration of Spectral Multiplexing Data
- AI object segmentation
- Leverage cell neighborhood and dimensionality reduction analysis to extract unique insights from your experiments

## Case Study Overview

Sample	Coronal mouse brain section
Task	3D channel registration, Segmentation, Dimensionality reduction analysis (tSNE), Cell neighborhood analysis
Results	Analysis of synaptic marker distribution and cell profiling in different brain anatomical regions
System	ZEISS LSM 980, Akoya Phenocycler
Software	ZEISS arivis Pro

## Introduction

Neuronal connectivity is the fundamental basis of brain function, allowing for the integration of information from multiple sources and the generation of complex behavior. The human brain contains an estimated 100 billion neurons, and each neuron can form synaptic connections with thousands of other neurons. Synapses are fundamental building blocks of neural circuits that underlie brain function and behavior. They form specialized junctions between neurons that allow for the transmission of information via electrochemical signals.

A synapse is composed of several components, including the presynaptic terminal, synaptic cleft, and postsynaptic terminal (Figure 1). The presynaptic terminal is located at the end of the axon and contains vesicles that store neurotransmitters. When an action potential reaches the presynaptic terminal, the vesicles fuse with the membrane, releasing the neurotransmitters into the synaptic cleft. The neurotransmitters then bind to receptors on the postsynaptic terminal, triggering a response. The specialized region of the presynaptic terminal where the vesicle docking, fusion and release happens is called the active zone.

The distribution of synapses plays a critical role in neuronal communication, learning, memory, perception, and cognition (Chen et al., 2018). Changes in the distribution of synapses, particularly in disease and aging, can profoundly affect brain function and behavior (Suedhof, 2018).

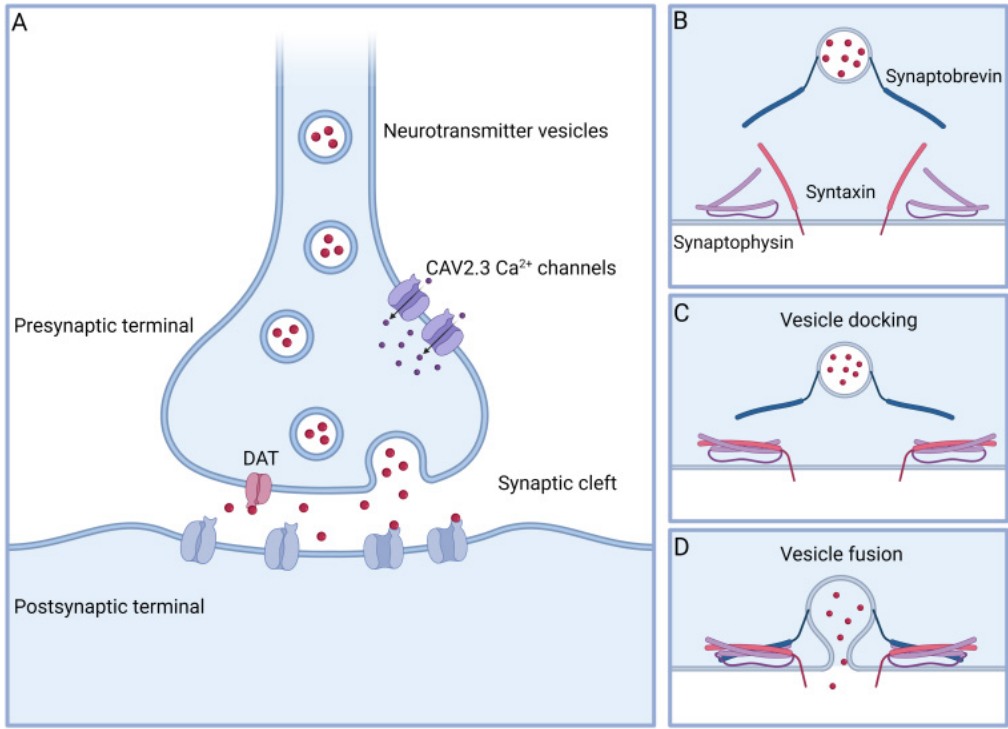


**Figure 1:** Schematic of antibody internalization and endolysosomal trafficking. The antibody (or other type of molecule) binds a plasma membrane-associated receptor. It is endocytosed into a membrane-bound vesicle and trafficked to a sorting endosome, where it can be recycled to the plasma membrane, transported to the Golgi, or retained as the compartment matures into a late endosome (note that these are Rab7a-positive). Late endosomes further mature into multivesicular bodies prior to fusion with a lysosome, which forms an endolysosome.

In this case study, the expression of an extensive list of pre-synaptic markers in mouse brain was analyzed. A region of interest (ROI) spanning three areas of the brain, the cortex, corpus callosum and striatum, was selected for imaging and analysis (Figure 2).

The cortex is a region of the brain that is highly interconnected, with each neuron forming connections with thousands of other neurons. The cortex is critical for various cognitive functions, including perception, attention, language, and memory. The corpus callosum is a large bundle of nerve fibers that connects the two hemispheres of the brain, allowing for communication and integration of information between the two hemispheres. The striatum is a region of the brain that is important for motor control and reward processing. The striatum is divided into two main compartments known as the striosome and matrix compartments, which have different patterns of connectivity and gene expression (Basile et al., 2021; Bamford and Bamford, 2019). Striosomes are small, oval-shaped clusters of neurons that are embedded within the matrix compartment of the striatum, characterized by their unique expression profile.

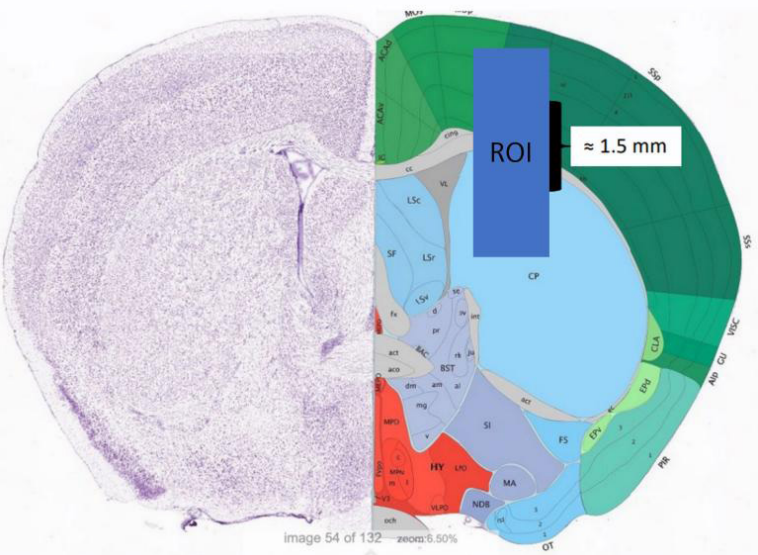


**Figure 2:** Coronal brain slice. The Region of Interest (ROI) is the area imaged and analyzed.

### List of pre-synaptic markers

A description of the markers for this case study is described in Figure 3. In Figure 1 you can see a simplified version of the localization of some of these proteins in the active zone of the synapse.

Marker	Protein Role
Bassoon	Large presynaptic protein involved in neurotransmitter release
Piccolo	Large presynaptic protein involved in neurotransmitter release
Synaptophysin	Transmembrane protein found in synaptic vesicles containing neurotransmitters
Syntaxin	Transmembrane protein found in the presynaptic active zone
CAV2.3	CAV2.3 is involved in the release of neurotransmitter vehicles in GABAergic neurons
CXCL12	Chemokine expressed by glial and neuron cells, important in supporting neuronal function and plasticity
DAT	Dopamine transporters (DAT) protein responsible for dopamine reuptake in the synaptic cleft
GAD67	Glutamic Acid Decarboxylase (GAD) responsible for the synthesis of the neurotransmitter gamma-aminobutyric acid (GABA)
NeuN	NeuN is a neuron-specific nuclear protein
GFAP	Glial Fibrillary Acidic Protein is expressed in astrocytes
MAP2	Microtubule associated protein 2, involved in the regulation of microtubule dynamics

**Figure 3:** Definition of markers used in the analysis.

## Material and Methods

The coronal brain tissue section (Figure 2) used in this case study was obtained from a 10-month-old adult mouse from an NGS background.

### Staining

Cyclical staining of the tissue section was accomplished with the Akoya PhenoCycler system (formerly CODEX®). The imaging was performed with the ZEISS LSM 980 confocal microscope using the ZEN acquisition software. The staining and imaging rounds were synchronized through custom macros written in the ZEISS ZEN “macro” environment (based on python code), and a script provided by Akoya (also written in python). Please contact ZEISS for more details on how to implement the interface between a ZEISS Imaging System based on ZEN and the Akoya PhenoCycler.

For this application, ten rounds of hybridization and imaging were implemented, with subsequent stripping and washing in between rounds. Two blanks were acquired at the beginning and end of the session to acquire background controls. In each cycle, DAPI staining was included and was used as a reference and fiducial channel for the downstream image alignment, registration, and analysis. In each cycle, three other fluorescent markers were included (Figure 4), an Alexa Fluor 488 tagged marker, an Alexa Fluor 555 marker, and an Alexa Fluor 647 marker.

To image the brain slice, a z-stack was set up for a region of 4x9 tiles which corresponds to an area of 1100x497x12  $\mu\text{m}$  in size. The ZEISS 63x Plan-Apochromat 1.4 N.A. oil immersion objective was used. This generates a pixel size of 70 nm. The z-step size for the z-stack was 0.3  $\mu\text{m}$ . These dimensions were optimal to achieve the full resolution improvement possible utilizing the ZEN LSM Plus processing feature for confocal data. LSM Plus utilizes a Wiener filter-based deconvolution to improve the resolution of the confocal data by 1.4x over what is traditionally obtained using a 1 A.U. pinhole for acquisition. LSM Plus additionally improves the overall signal-to-noise ratio of the images, and therefore, no averaging was needed. After acquisition, the images were background corrected using the smoothed images acquired from the blank cycles.

	<b>488</b>	<b>550</b>	<b>647</b>
Cycle 1		Blank	
Cycle 2	SYNAPSIN-RX001	CD31-RX002	CD68-RX003
Cycle 3	NESTIN-RX001	SYNTAXIN-RX005	NEUROLIGIN1-RX006
Cycle 4	ALPHA SYN-RX004	PAX6-RX041	SYNAPTOPHYSIN-RX021
Cycle 5	DAT-RX016	BASSOON-RX014	DARPP32-RX024
Cycle 6	SYNAPTOBREVIN-RX010	PICCOLLO-RX020	NEUN-RX027
Cycle 7	GFAP-RX007	GAD67-RX029	CAV2.3-RX042
Cycle 8	NEUROFILAMENT-RX022	CXCL12-RX017	TH-RX045
Cycle 9	SNAP25-RX037	MAP2-RX023	S100B-RX036
Cycle 10		Blank	

**Figure 4:** Staining cycles and marker combinations.

In these complex multiplexing applications with multiple rounds of staining, it is often the case that only certain markers are needed in a given analysis set. For the analysis shown in the publication above and the example shown here, the following markers were combined into a final 3D multiplex data set:

Markers for Synaptic Analysis	Markers for Cell Analysis
GFAP	Bassoon
MAP2	CAV2
Bassoon	CXCL12
Piccolo	DAT
Syntaxin	GAD6
Synaptobrevin	NeuN
Synaptophysin	

**Figure 5:** Markers used for the different types of analysis.

## Software Processing

### Registration of Multiplexing Data

Image registration is the process of transforming different sets of data to overlay images from different experiments, taken at different time points, positions, or angles, or with different imaging modalities. The registration algorithm attempts to discover the matching areas in the corresponding images and align them together in a pairwise manner. For the multiplexing experiments, we used the nuclei staining (DAPI) in each of the staining cycles to register the subsequent multiplexing rounds to the first staining cycle. This method is applicable both to 2D and 3D images.

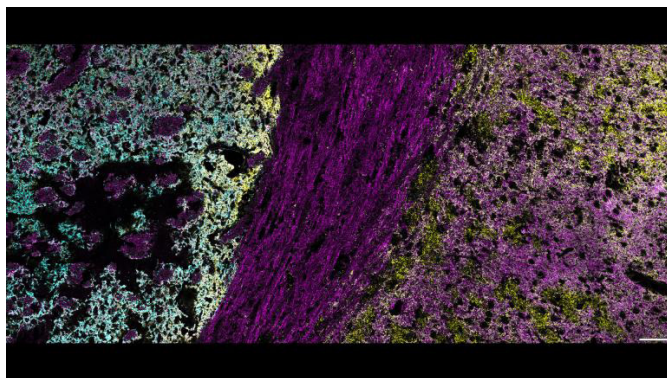


**Figure 6:** Three marker overlay, DAT (blue), Synaptophysin (yellow) and Syntaxin (magenta)

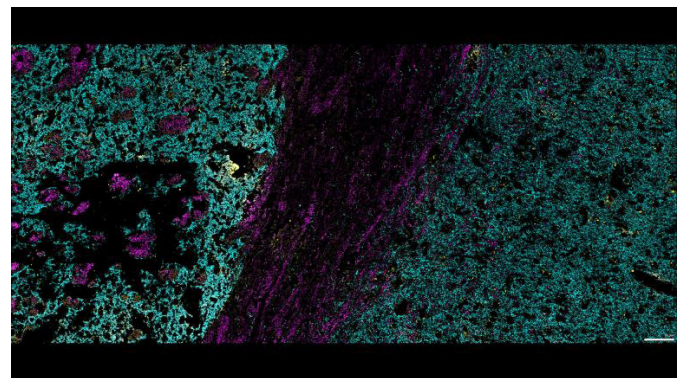


**Figure 7:** Three marker overlay, Bassoon (blue), Synaptobrevin (yellow) and Piccolo (magenta)

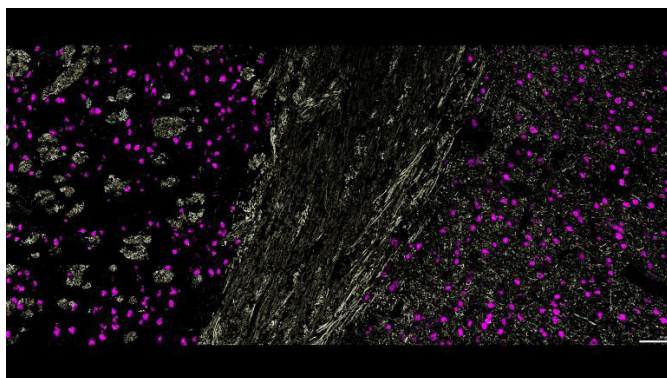


**Figure 8:** Three marker overlay, CXCL 12 (blue), MAP2 (yellow) and NeuN (magenta)

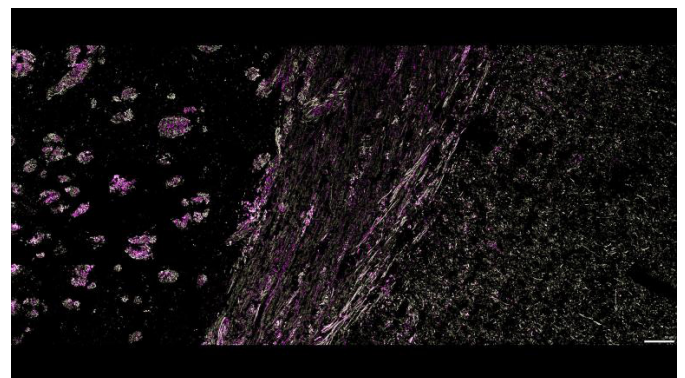


**Figure 9:** Three marker overlay, CXCL 12 (blue), MAP2 (yellow) and Piccolo (magenta)

The registration was performed in a tile-wise manner using a custom python script integrated in ZEISS arivis Pro. The DAPI signal in the first staining cycle was used as the reference image, and the DAPI staining from the second and the following staining cycles were used as the 'moving' or 'warping' images and were registered to the reference DAPI image using rigid transformations (rotation and translation). The obtained transformation parameters were applied to all other channels in the corresponding staining cycle. The registration python script and its implementation are available and described in this application note.

This step and the following analysis were performed in ZEISS arivis Pro version 4.1.1.

In the following, tiles, containing all staining cycles (13 channels in total, after the duplicate DAPI channels were removed) were assembled and merged in the final image using the Tile Sorter tool in ZEISS arivis Pro.

### Segmentation of anatomical regions

The ROI contained the three adjacent anatomical brain regions (cortex, corpus callosum, and striatum), with distinct morphologies and staining patterns. Specifically, the Bassoon staining was used as a marker to segment the striatum and cortex brain regions. Corpus callosum was segmented using the Image Math operator, as the area between the striatum and cortex. In addition, the striosomes were segmented separately, as regions of the striatum with a higher MAP2 expression. To accelerate the segmentation speed due to the dataset size, this part of the analysis was performed at 12.5% scale. The resulting segments were automatically scaled back to 100% image size in ZEISS arivis Pro (Figure 13).

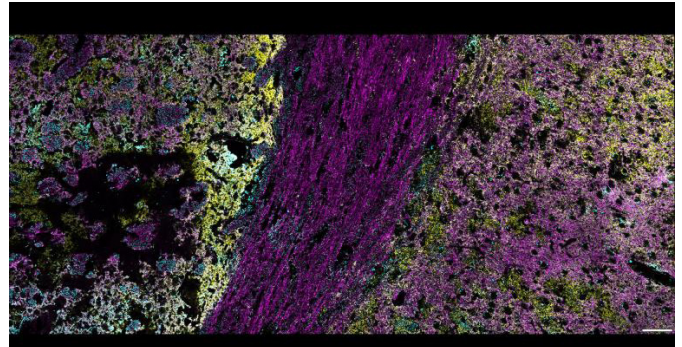


Figure 10: Three marker overlay, Synaptobrevin (blue), Synaptophysin (yellow) and Syntaxin (magenta)

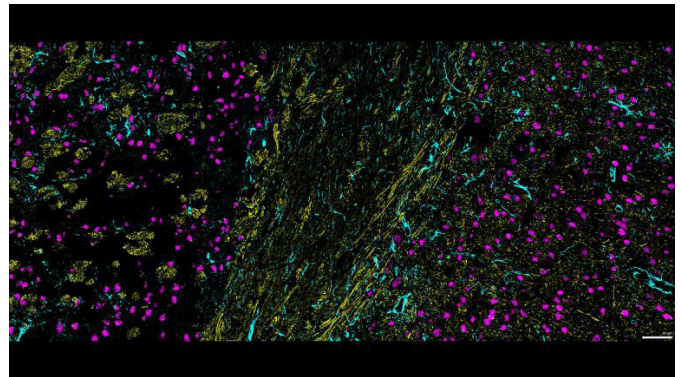


Figure 11: Three marker overlay, GFAP, MAP2 and NeuN

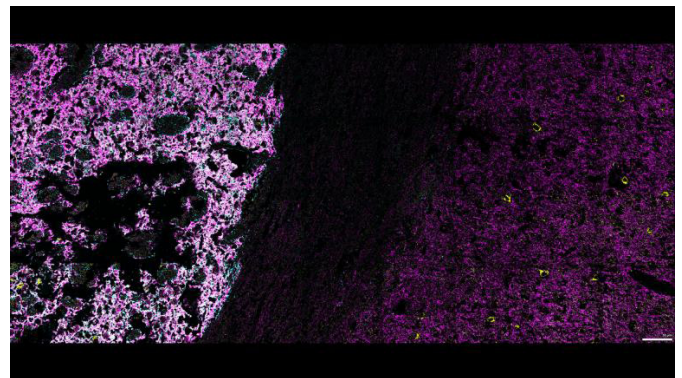


Figure 12: Three marker overlay, CAV2 (blue), GAD (yellow) and DAT (magenta)

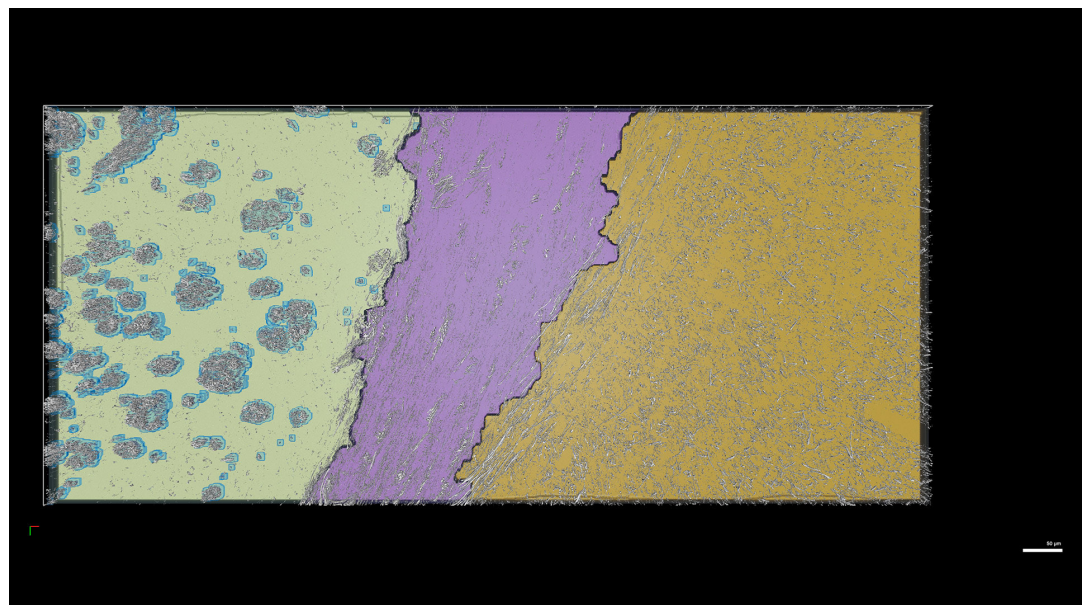


Figure 13: Segmentation of anatomical regions. Striatum is labelled in yellow, striosomes in blue, corpus callosum in violet, and cortex in orange.

## Segmentation of cells

Each cell nucleus was segmented using the Cellpose instance segmentation deep learning algorithm integrated in ZEISS arivis Pro. The DAPI staining of the first staining round was used for the segmentation with the pre-trained 'Nuclei' model, followed by a filtering step with Instance Segmentation AI (Figure 14).

Cellpose references:

[Stringer, C, Wang, T, Michaelos, M, and Pachitariu, M "Cellpose: a generalist algorithm for cellular segmentation", Nature methods, 2021](#)

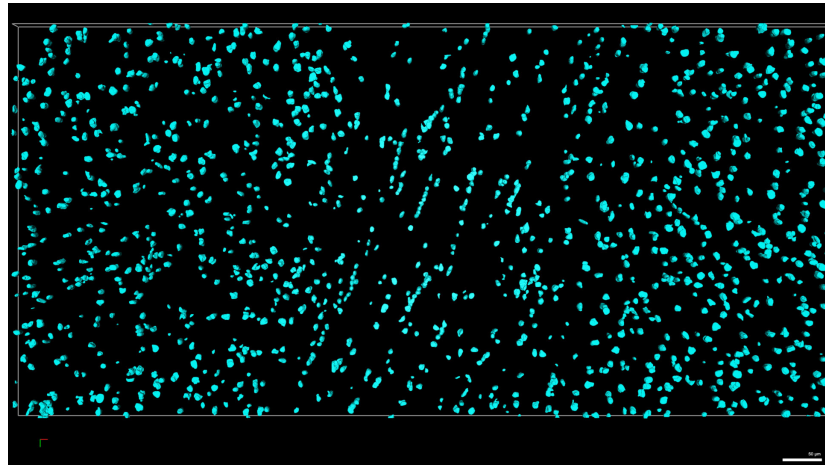


Figure 14: Segmentation of cell bodies.

[Pachitariu, M. and and Stringer, C. "Cellpose 2.0: how to train your own model", Nature methods, 2022](#)

## Segmentation of neurofilaments and astrocytes

For the MAP2 filament segmentation, the signal was enhanced by applying the Filaments Shape Detection algorithm in the ZEISS arivis Pro set to the corresponding filament diameter. The filament-enhanced image was averaged together with the original data.

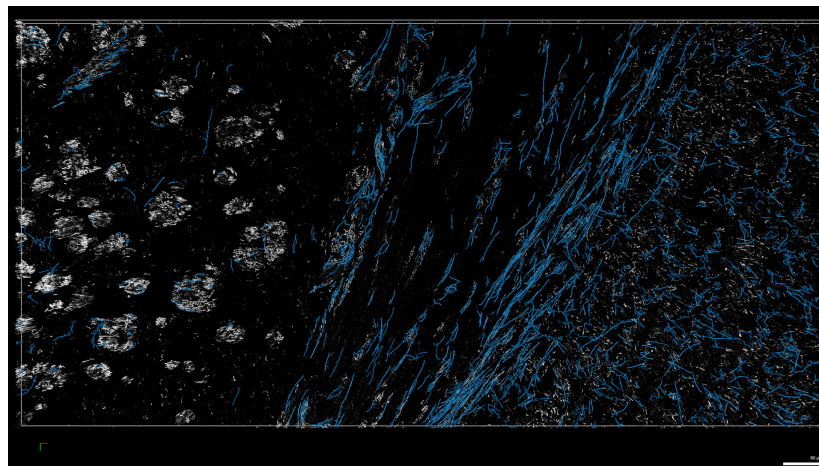


Figure 15: Segmentation of MAP2 filaments.

Next, the microtubule filaments were segmented using the Neurite Tracer, and specifically the Probabilistic Reconstruction algorithm. This operator determines the local tubularity of the image data. This tubularity map is then searched for seed points. Starting from seed points, using a probability function, trace parts are detected. These trace parts are then merged to create the complete trace [reference] (Figure 15).

[Miroslav Radojevic, and Erik Meijering "Automated Neuron Reconstruction from 3D Fluorescence Microscopy Images Using Sequential Monte Carlo Estimation", Bioinformatics, 2019](#)

Astrocytes have a strong high-contrast signal, distinct morphology, and are strongly labelled by the GFAP marker. The segmentation was performed in one step using the Neurite Tracer Probabilistic reconstructor, similar to the MAP2 segmentation. To compute the distances from the synapses to the neurofilaments and microglia, these two trace types were converted into segment - type objects (Figure 16).

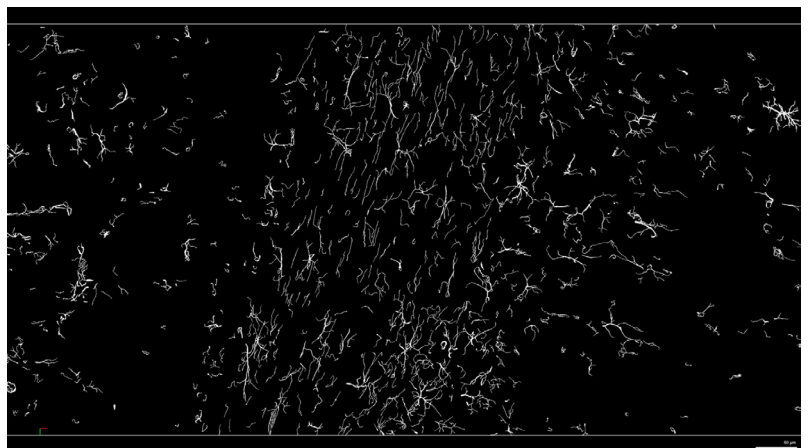


Figure 16: Segmentation of GFAP, labeling astrocytes.

## Segmentation of synapses

For segmentation of the synaptic puncta, the four pre-synaptic markers were available (Piccolo, Syntaxin, Synaptobrevin, and Synaptophysin). In the absence of the post-synaptic marker or the pan-synaptic staining, the four channels with the pre-synaptic markers were averaged. For this, the intensities in each channel were measured separately on the original data. Initially, the images were normalized to 1-99% of their intensities. By normalizing the images to 1-99% of their intensities, the brightest and darkest 1% of pixels are saturated, while the remaining pixels are rescaled to fit within the remaining 98% of the intensity range. This helps to enhance the contrast between different structures and features in the image, making it easier to identify and segment specific structures such as synaptic puncta.

Then, the background was corrected by subtracting a blurred version of the image from the original data for each channel separately. The blur diameter was set to 100 pixels. Next, to enhance the puncta in the image, a top-hat filter ('Preserve bright objects' operator in ZEISS arivis Pro) with a disk structural element of 8 pixels was applied. Then, the data from the four pre-synaptic markers was averaged together and segmented using the Blob finder operator. This algorithm includes a combination of automatic seed finding based on structural information of an object map, and a watershed algorithm. This operation uses the Gaussian scale to find the object seeds and a watershed algorithm to identify object boundaries.

Finally, the segmented synapse objects were filtered by size with the lower limit of 5 voxels, corresponding to 70 nm<sup>3</sup>.

## Allocation of cell and synapses to anatomical regions (process + summary table)

Once the segmentation for all components was complete, the final pipeline consisted of importing the anatomical regions, synapses, GFAP and MAP segments. Due to the very large number of synapses (1.7M), a new custom python operator was implemented, to randomly sub-sample 10 thousand synapses out of the total number of 1.7M synapses, detected in the image [The script and the application note is available here]. The subsetted synapses were allocated into the three anatomical structures (cortex, corpus callosum, and striatum), as well as striosomes.

In Figure 17, the number of cells, and volume for each anatomical region is summarized. Additionally, the total number of synapses and the percentage found in each region is also displayed.

Anatomical Regions	Number of Cells	Volume	Synapses
Cortex	845	2,791,611 $\mu\text{m}^3$	42.69%
Striatum (incl. Striosomes)	719	2,454,340 $\mu\text{m}^3$	34.51%
Corpus callosum	296	1,328,432 $\mu\text{m}^3$	22.8%
Total	1825	6,574,383 $\mu\text{m}^3$	1.1M

**Figure 17:** Summary table of the segmentation results.

## Reduced dimensionality analysis

To visualize this very complex dataset, t-SNE (t-distributed Stochastic Neighbor Embedding) analysis was performed. This is a nonlinear dimensionality reduction technique used to visualize high-dimensional data in low-dimensional space. It achieves this by representing each data point as a probability distribution in the low-dimensional space and minimizing the difference between the pairwise similarities of the high-dimensional data and the pairwise similarities of the low-dimensional representation.

In this case study, dimensionality reduction analysis was conducted twice, once for the cells and once for the synapses. For the synapsis analysis, 28 features (XYZ coordinates, mean intensity levels, signal-to-noise ratios and integrated densities from six channels and puncta volume, their randomly subsampled neighborhood densities, and distances to GFAP and MAP2, and their anatomical regions [cortex, corpus callosum, striatum, striosomes]) for each synaptic puncta were used as the input to t-SNE. Only the 10K subsetted synapses were used for the expression profile analysis. For the cell analysis, 27 features were analyzed (XYZ coordinates, mean intensity levels, signal-to-noise ratios and integrated densities from six channels, their neighborhood densities, and distances to GFAP and MAP2, and their anatomical regions [cortex, corpus callosum, and striatum]).

To ensure that the visualization is robust to differences in scale and variability across the different features, the features were pre-processed by being log-transformed and normalized to have a standard deviation of one and minimum of zero before applying t-SNE. The logarithmic transformation reduces the effects of extreme values or outliers. This normalization is done to transform the data so that it has a standardized scale across different features, which will make their visualization more accurate and efficient. Standard deviation is a measure of how spread out the data are, with higher values indicating more variability. By setting the standard deviation to one, the data are rescaled so that each feature has a similar level of variability. Additionally, by setting the minimum value to zero, the data are shifted so that the lowest value for each feature is zero, which can simplify the interpretation of the data and make it easier to compare across different features. The t-SNE analysis was performed using scikit-learn 1.3.0 in Python 3.11.4 with the exact method, perplexity parameter equal to 40 and 5000 iterations.

# Results

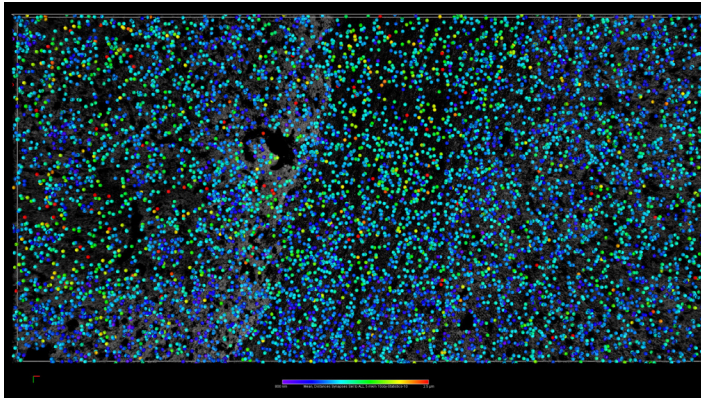


**Figure 18:** Synaptic density. Visual representation of the 10K randomly selected synapses, color-coded by their distance to their five closest neighbors from the total synaptic pool.

## Characterization of synaptic connectivity

### Spatial mapping of synaptic density and connectivity

To assess the distribution of synapses throughout the brain regions, the average distance between each of the subsetted synapses (10K) and their five nearest neighbors from the total synaptic pool was calculated. The resulting measurements were used to color-code individual synapses with blue indicating a shorter distance and red indicating a longer distance to their immediate neighbors (Figure 18). Based on this analysis, the synaptic density is relatively uniform across different anatomical regions of the brain.

Astrocytes are known to have a crucial role in regulating synaptic function and plasticity, and their processes are often located near synapses. To investigate the interactions between astrocytes and synapses, the distance between synaptic puncta and astrocytes was analyzed and visualized in Figure 19. The results showed that most synapses in the corpus callosum were in close contact with GFAP. Interestingly, the distribution of GFAP-positive cells in the corpus callosum, as depicted in Figure 17, demonstrated a significant population of GFAP cells in the region, further supporting the notion of high glial and synaptic interactions in corpus callosum. Additionally, it has been reported that the density of astrocytes is greater in the white matter, such as the corpus callosum, compared to the grey matter, such as the cortex and striatum (Oberheim et al., 2009). However, clusters of cells in the cortex and striatum were also found to have a high proximity to GFAP filaments, with striatal clusters primarily located within the striosomes.

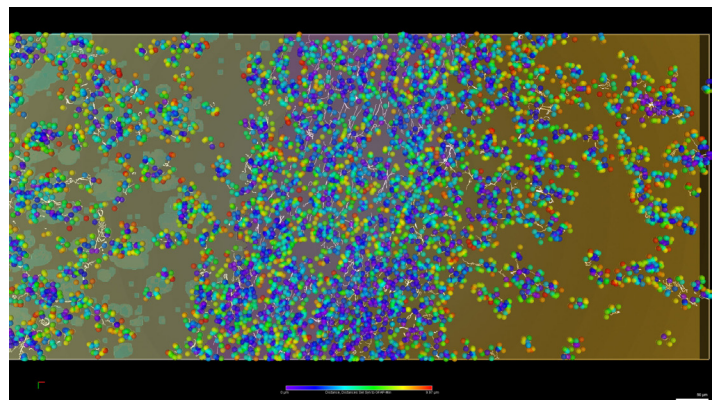


**Figure 19:** Synaptic proximity to GFAP. Visual representation of the subsetted synapses, color-coded by their distance to the nearest GFAP filament. The objects with a distance over 200  $\mu\text{m}$  were removed.

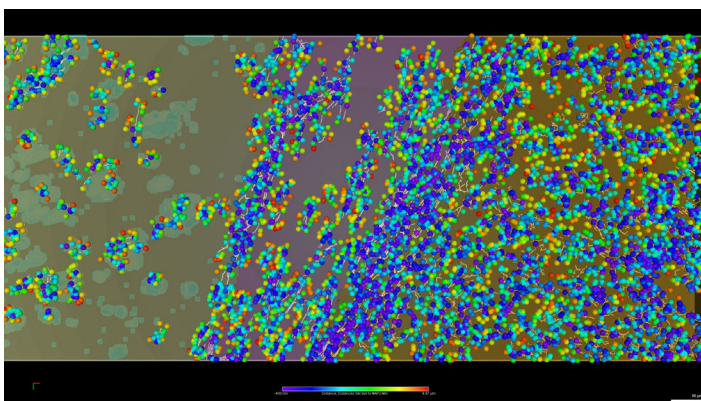


**Figure 20:** Synaptic proximity to MAP2. Visual representation of the subsetted synapses, color-coded by their distance to the nearest MAP2 filament. Objects with a distance over 200  $\mu\text{m}$  were removed.

To investigate the spatial relationship between synapses, dendrites, and astrocytes, the distance between the subsetted synapses and the nearest MAP2 was measured. MAP2 is primarily expressed in dendrites and plays a critical role in stabilizing microtubules (Sanabria, Suárez, & Rodríguez-Moreno, 2004). The distance of a synapse to MAP2 can serve as an indicator of the synapse's location within the dendritic tree. Synapses that are situated closer to MAP2 are more likely to be situated on dendrites, whereas those that are further away from MAP2 may be positioned on the cell body or axon of the neuron. It was observed that most synapses in the corpus callosum and cortex were in very close contact with MAP2, as shown in Figure 20.

Notably, the striatal synaptic clusters in close contact with MAP2 filaments are either within or adjacent to striosomes, and not in the striatal matrix. Additionally, most cortical synapses are in very close contact with MAP2 filaments.

## Topography of synaptic protein expression

To visualize the distribution of synapses in the low dimensionality space and reveal relationships between the different markers and their expression level distribution, t-Stochastic Neighbor Embedding (t-SNE) was used as described in section 4.7.

First, a t-SNE visualization was generated to illustrate the distribution of individual synaptic puncta in the low-dimensional space based on the similarity of their anatomical location. In this t-SNE visualization, each spot in the final plot corresponds to a single synaptic punctum. The positioning of the spots in the plot is determined by the similarity of the puncta based on the anatomical region, with synapses in the same brain region clustered together and synapses in different brain regions clustering further apart. The allocation of each synapse to its respective anatomical region was determined through the Compartmentalization analysis as part of the ZEISS arivis Pro pipeline (Results 5). The resulting t-SNE plot clearly shows clustering of the synapses into four distinct large sub-groups, each corresponding to a specific anatomical region as captured in the tissue section (Figure 21). In each of these plots, the synapses belonging to a specific region (e.g., Figure 21, Panel A – Corpus callosum) are distinguished in yellow, while the remaining synapses in the same plot are labeled in purple.

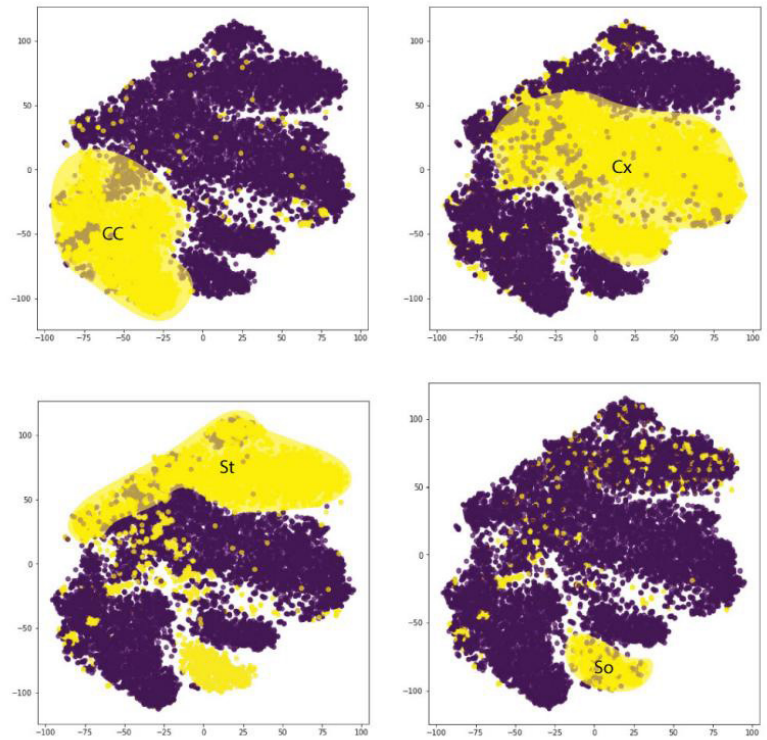


**Figure 21a:** Brain region clustering in the reduced dimensionality space. Each spot represents an individual synapse

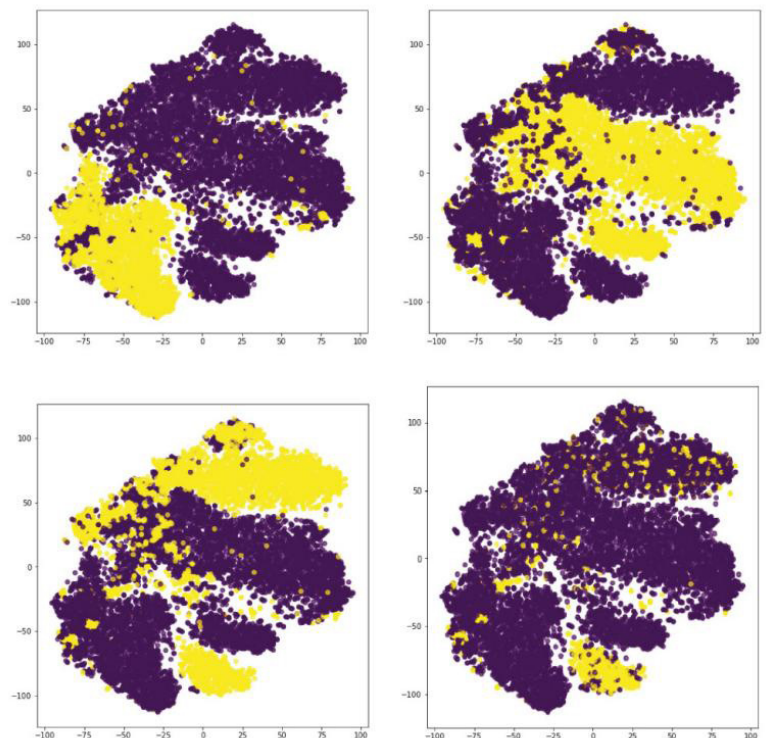


**Figure 21b:** Brain region clustering in the reduced dimensionality space. Each spot represents an individual synapse

The active zone is a specialized region of the pre-synaptic terminal of a neuron that is responsible for the regulated release of neurotransmitters into the synaptic cleft. It is composed of a complex network of proteins that work together to ensure the efficient and precise release of neurotransmitters in response to incoming signals. The expression patterns of presynaptic markers syntaxin, synaptobrevin and synaptophysin, known to be strongly involved in the formation, maintenance and function of the active zone were evaluated (Figure 22). The expression of all three presynaptic markers is higher in the cortex and striatum regions, an observation also made by published studies (Nagy and Carter, 1994; Darios et al., 2010; Vos et al., 2010). The higher expression of these markers in the cortex and striatum could be related to their important roles in motor control and cognitive function (Luo et al., 2005).

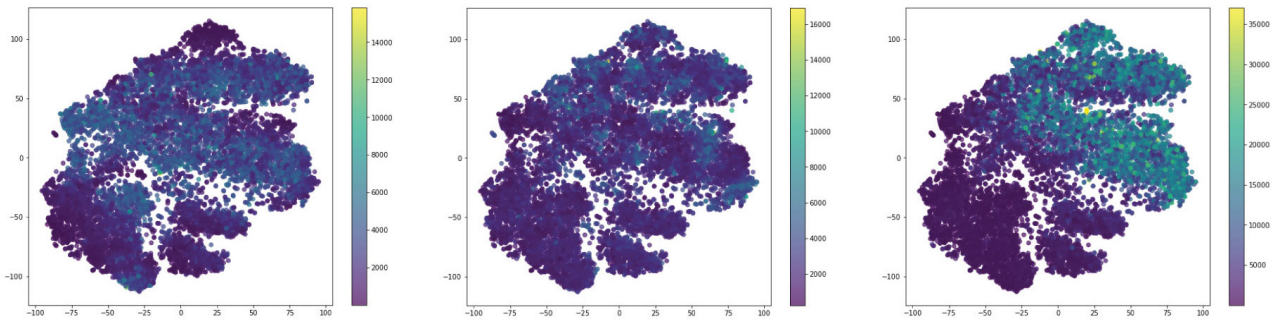


**Figure 22a:** Expression of Syntax, Synaptobrevin and Synaptophysin in the reduced dimensionality space.

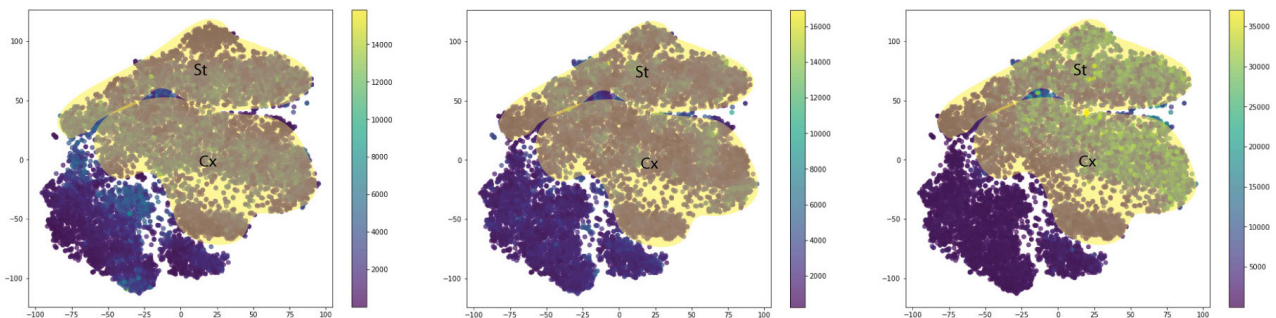


**Figure 22b:** Expression of Syntax, Synaptobrevin and Synaptophysin in the reduced dimensionality space.

In Panels A and B in Figure 23, both Piccolo and Bassoon are expressed at low levels in all synapses, as expected. Piccolo has a higher expression in the corpus callosum and the striosomes, whereas Bassoon is expressed at higher levels in the cortex and striatum. This mutual exclusivity in the areas of the higher expression of these proteins is unexpected, since they belong in the same protein family and are considered to be functioning together at the synapsis.

MAP2 expression was evaluated across the brain regions (Figure 23). Other than the dendritic tree, MAP2 is also found in the presynaptic terminal, where it plays a role in the regulation of neurotransmitter release (Kawasaki et al., 2010). As expected, MAP2 is homogeneously expressed throughout the brain regions, with slightly higher expression in the corpus callosum and the striosomes. This observation is in line with previous results that show that MAP2 expression are enriched in the corpus callosum and in the striosomes (Figure 15).

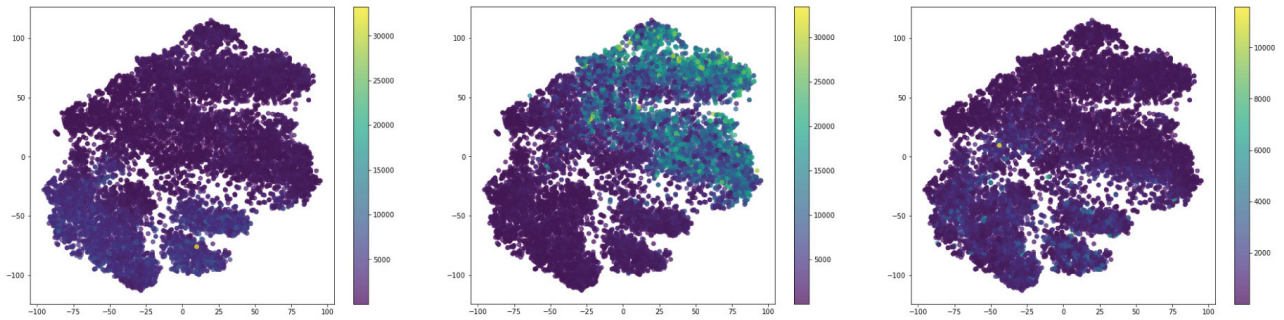


Figure 23a: Expression of Piccolo, Bassoon and MAP2 in the reduced dimensionality space.

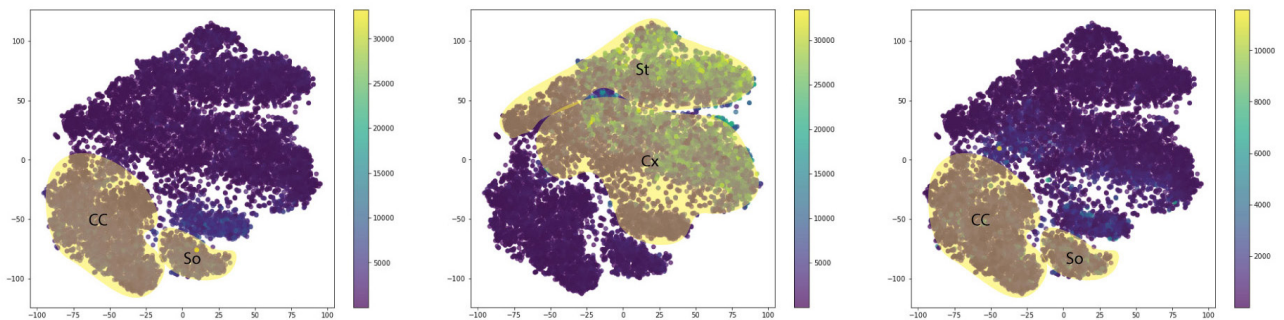
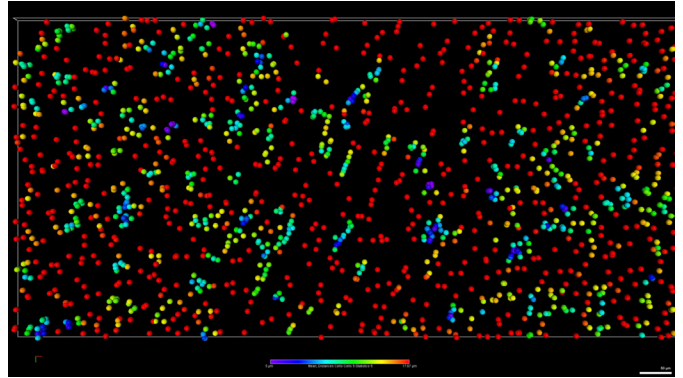


Figure 23a: Expression of Piccolo, Bassoon and MAP2 in the reduced dimensionality space.

## Brain cell profiling

### Spatial mapping of cell body density and connectivity

To unveil information about the organization of cells within the tissue as well as neighboring cell-cell interaction, a cell neighborhood density analysis was performed. The latter is a measurement of the number of cells within a certain distance or radius from a given cell or structure in the tissue. A high cell neighborhood density indicates that cells within the tissue are closely packed together and may be interacting with each other frequently. On the other hand, a low cell neighborhood density may suggest that the cells are more dispersed and may be less functionally connected to each other. The density of the cells was evaluated by calculating their distance to the nearest five neighboring cells by the distance operator within ZEISS arivis Pro. Notably, the cell population analyzed includes all brain cells identified by DAPI, such as neurons, astrocytes, oligodendrocytes, etc. To visualize these results, the cells were color-coded based on distance, with blue suggesting smaller distance and higher density and red longer distance and lower density (Figure 24). Overall, the cell density is homogeneously low, since most cells are color-coded red.



**Figure 24:** Cell density. Digital reconstruction of the cell bodies represented as objects, color-coded by their distance to their 5 closest neighbors.

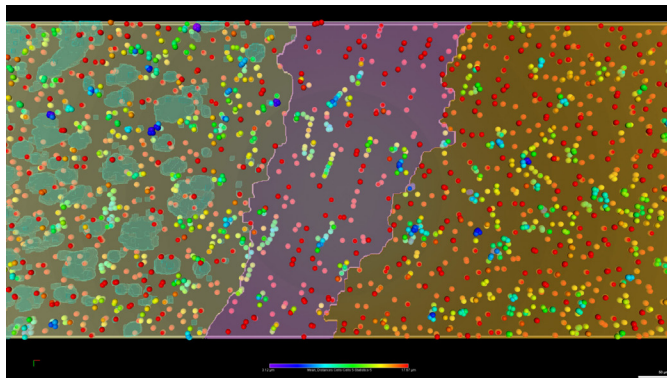


**Figure 25:** Cell density overlaid with brain regions. Digital reconstruction of the cell bodies represented as objects, color-coded by their distance to their five closest neighbors.

However, a subset of cells in clusters can be identified in all brain regions. In the cortex and the striatum, the cell clusters are round, whereas in the corpus callosum the clusters form strings of cells (Figure 25). The cell clusters in the striatum are adjacent to, but not contained within, the striosomes (Figure 25), which is complementary to the previous observation that the striosomes contain synapses (Figure 19, Figure 20).

To evaluate if the clustered or singular brain cells were in closer contact with astrocytes, the distance of the cells to GFAP was calculated. As visualized in Figure 26, most single cells in the corpus callosum and cortex are in close contact with astrocytes. However, the string clusters in corpus callosum are further away from GFAP filaments. Additionally, there are patches of cells in the striatum that are the furthest away from astrocytes.

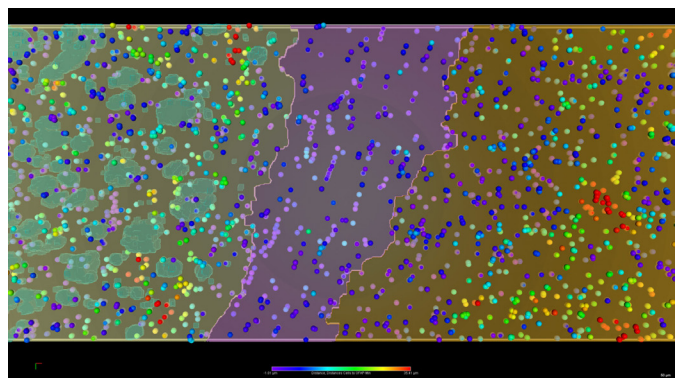


**Figure 26:** Cell proximity to GFAP. Digital reconstruction of the cell bodies represented as objects, color-coded by their distance to GFAP signal.

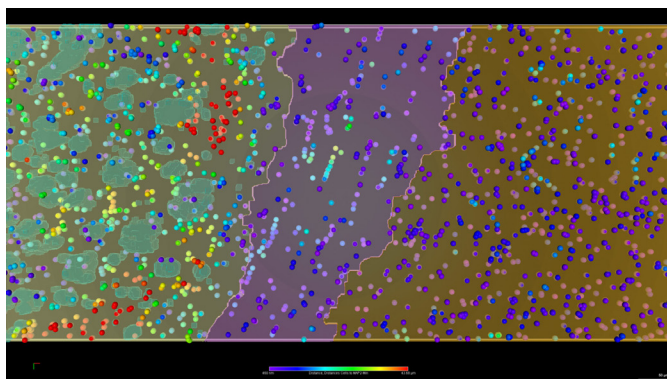


**Figure 27:** Cell proximity to MAP2. Digital reconstruction of the cell bodies represented as objects, color-coded by their distance to MAP2 filaments.

To assess the proximity of cells to dendrites, the distance to MAP2 filaments was calculated (Figure 27). The cells of the corpus callosum and the part of the cortex that is adjacent to it have the tightest association with MAP2. The striatal cells are the furthest apart from the MAP2 filaments, which is expected as the majority of the striatal MAP2 filaments are found in the striosomes (Figure 15) that are void of cells (Figure 25).

## Topography of cell protein expression

For the cell dimensionality reduction analysis, first the t-SNE visualization was generated to illustrate the distribution of individual cells in the low-dimensional space based on their localization in reference to the identified anatomical regions (Figure 28). In each of these plots, the cells belonging to a specific region (e.g., Panel A – Striatum) are distinguished in yellow, while the remaining cells in the same plot are labeled in purple. The striosomes were not defined as a separate region, as from previous analysis they appear to be void of cells (Figure 25).

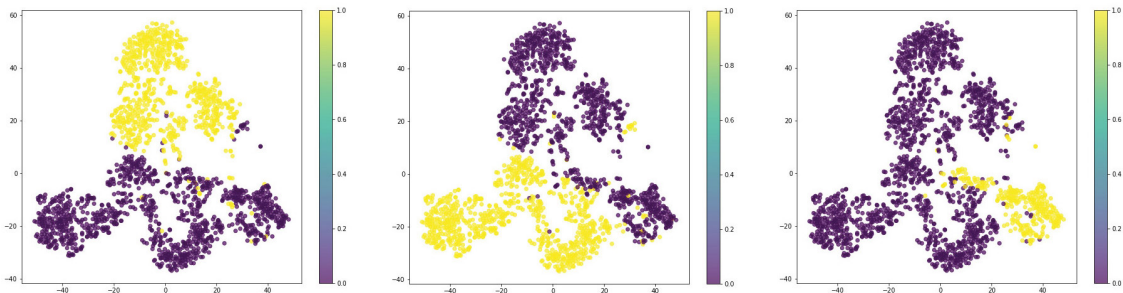


Figure 28a: Brain region clustering in the reduced dimensionality space. Each spot represents an individual cell

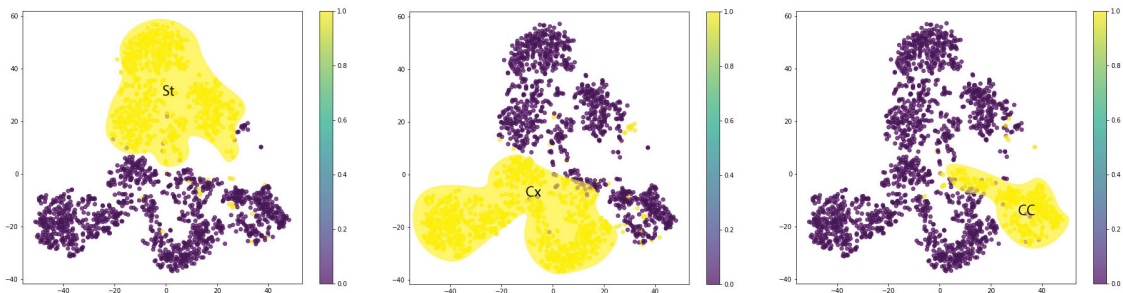


Figure 28b: Brain region clustering in the reduced dimensionality space. Each spot represents an individual cell

Since the cell population analyzed is a mixture of brain cells, cell markers specific for different cell subsets were evaluated (Figure 29). NeuN is a protein expressed in the nuclei of most mature neurons and can be used to identify the neural cells in the t-SNE analysis. As seen in Figure 29, panel A, NeuN expression is enriched in the cortex and striatum, and lower in the corpus callosum. This is in line with the general understanding that the vast majority of neurons is found in parts of the cortex and striatum, whereas the corpus callosum contains very few neuronal cell bodies and more astrocytes. The latter are the key producers of CXCL12 in the brain regions. The expression of CXCL12 is found in almost complementary regions with NeuN, specifically in the corpus callosum, and the cells of cortex expressing the lowest levels of NeuN (Panel B, Figure 29). Bassoon is traditionally known as a presynaptic marker; however, it can also be detected in the cell body of neurons (Hirano et al., 1999). As expected, Bassoon is expressed homogeneously across the brain regions (Panel C, Figure 29). Intriguingly, areas with slight enrichment of Bassoon expression, appear to coincide with the respective CXCL12 ones. This could be due to the known role of both proteins in neural plasticity.

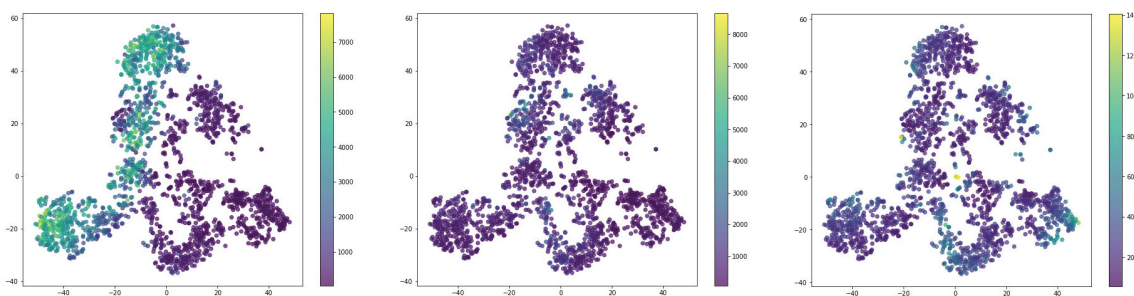


Figure 29a: Expression of NeuN, Bassoon and CXCL 12 in the reduced dimensionality space.

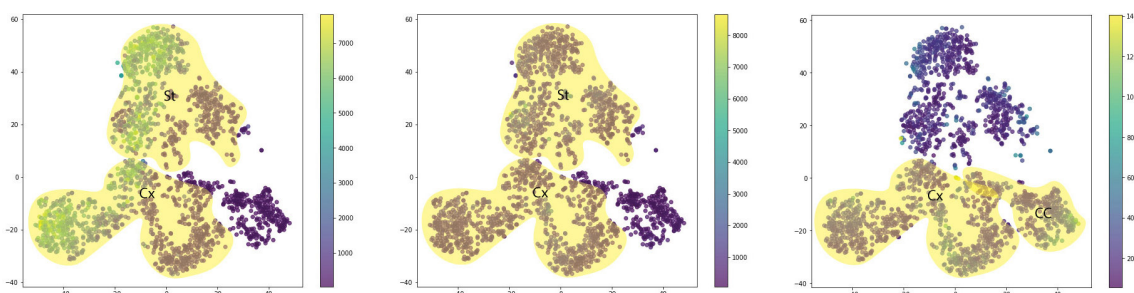
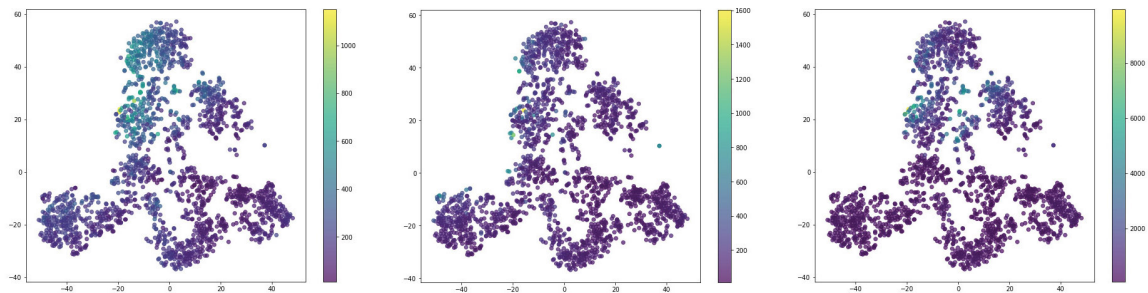


Figure 29a: Expression of NeuN, Bassoon and CXCL 12 in the reduced dimensionality space.

To gain insight into the regulation of neurotransmitter signaling in the brain, the expression profile of CAV2.3, GAD and DAT was evaluated. CAV2.3 and GAD are key markers of GABAergic neurons, with GAD being involved in the production of GABA from glutamate, and CAV2.3 being involved in regulating the release of GABA. As expected, both proteins are expressed in all brain regions (Panel A-B, Figure 30). However, the expression of both markers is enriched in the striatum, which is in line with previous studies that show that the striatum has a higher density of GABAergic neurons compared to the cortex (Tepper et al., 2010). The expression of DAT is also enriched in the striatal region (Panel C, Figure 30).

DAT is known to be expressed at higher levels in striatal neurons compared to other brain regions (Ciliax et al., 1995). DAT is a membrane protein that is responsible for the reuptake of dopamine from the synaptic cleft back into the presynaptic neuron, thereby regulating the levels of dopamine signaling in the brain. The striatum is a primary target of dopaminergic projections from the midbrain, and the high expression of DAT in striatal neurons is thought to play a crucial role in regulating dopamine signaling in this region.



**Figure 30a:** Expression of CAV2, DAT and GAD in the reduced dimensionality space

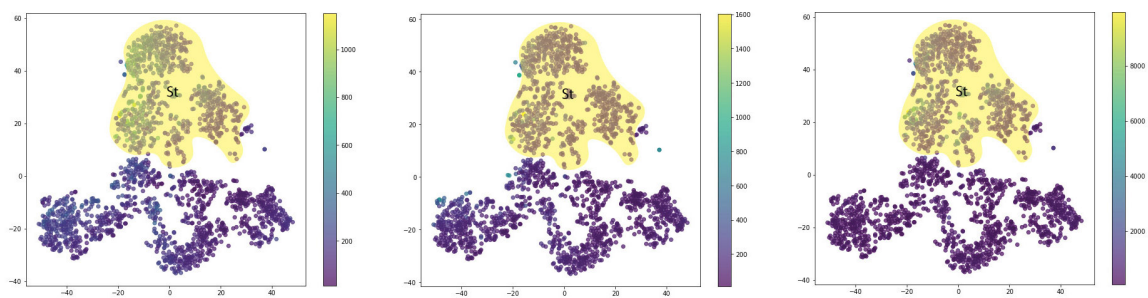


**Figure 30b:** Expression of CAV2, DAT and GAD in the reduced dimensionality space

## Summary

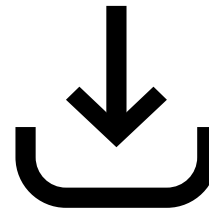
In this case study, we have demonstrated example analyses for 3D multiplexing spatial omics data based on cellular and synaptic markers in the mouse brain.

These examples can be used to design analyses for 3D registration of multiplexing data, the segmentation of objects using AI, and the cell neighborhood and reduced dimensionality analysis. The registration algorithm aligns images from different experiments, while segmentation and allocation of components enable the analysis of their distribution across different anatomical regions. Cell neighborhood analysis provides insights in cellular organization, whereas reduced dimensionality analysis using t-SNE helps visualize high-dimensional data in low-dimensional space. These steps were performed using ZEISS arivis Pro and custom python scripts, resulting in a comprehensive analysis of the complex dataset.

In this experiment, the spatial distribution and organization of synapses, cells, and astrocytes in different brain regions was investigated. Various observations were made regarding the density and distribution of cells and synapses in the mouse brain. The expression of various presynaptic markers and cell-specific proteins were also evaluated, and the intricate expression patterns were discussed. These analyses serve as a valuable blueprint for users to follow with their own three-dimensional spatial omics data. The techniques used in this study can be applied across a wide range of applications in neuroscience, cancer research, immunology, and single-cell analysis. By exploring cell heterogeneity and clustering, characterizing cell-cell interactions, and identifying biomarkers, these type of analyses can provide a deeper understanding of complex biological systems and disease mechanisms.



**Request the Trial Version  
of ZEISS arivis Pro**



**Download Case Study Files**

### References

- Darios, F., Wasser, C., Shakirzyanova, A., Giniatullin, A., Goodman, K., Munoz-Bravo, J. L., Raingo, J., Jorgacevski, J., Kreft, M., Zorec, R., Rosa, J. M., Gandia, L., Gutierrez, L. M., and Binz, T. (2010). Sphingosine facilitates SNARE complex assembly and activates synaptic vesicle exocytosis. *Neuron*, 68(2), 210-223. doi: 10.1016/j.neuron.2010.09.003
- Genoud, C., Quairiaux, C., Steiner, P., Hirling, H., Welker, E., & Knott, G. W. (2013). Plasticity of astrocytic coverage and glutamate transporter expression in adult mouse cortex. *PLoS One*, 8(2), e53553. doi: 10.1371/journal.pone.0053553
- Hirano, T., Okamoto, S., Shibato, T., Tanaka, K., & Shiosaka, K. (1999). Bassoon protein is localized at the presynaptic active zone in both excitatory and inhibitory synapses. *Journal of Neuroscience Research*, 58(1), 34-41
- Kawasaki, F., Mattson, M. P., & Jiang, M. (2010). Effects of amyloid-beta precursor protein on synaptic plasticity and neurotransmitter release are dependent on its distribution in the synapse. *Journal of Biological Chemistry*, 285(48), 37181-37190. doi: 10.1074/jbc.M110.149005
- Luo, L., & O'Leary, D. D. (2005). Axon retraction and degeneration in development and disease. *Annual review of neuroscience*, 28, 127-156.
- Nagy, J.I., and Carter, D.A. (1994). Purification and characterization of syntaxin and synaptobrevin, two nervous system-specific proteins that participate in synaptic vesicle fusion. *Journal of Neuroscience Research*, 38(2), 192-203. doi: 10.1002/jnr.490380209
- Oberheim, N. A., Takano, T., Han, X., He, W., Lin, J. H., Wang, F., ... & Goldman, S. A. (2009). Uniquely hominid features of adult human astrocytes. *Journal of Neuroscience*, 29(10), 3276-3287.
- Sanabria, H., Suárez, L. M., & Rodríguez-Moreno, A. (2004). Increase of dendritic spine density in hippocampal pyramidal neurons by activation of the group I metabotropic glutamate receptor subtype 5 (mGluR5). *Journal of Neuroscience*, 24(35), 8750-8758. doi: 10.1523/JNEUROSCI.2895-04.2004
- Südhof, T. C. (2012). The presynaptic active zone. *Neuron*, 75(1), 11-25. doi: 10.1016/j.neuron.2012.06.012
- Tepper, J. M., Tecuapetla, F., Koos, T., & Ibanez-Sandoval, O. (2010). Heterogeneity and diversity of striatal GABAergic interneurons. *Frontiers in neuroanatomy*, 4, 150
- Vos, J.P., Geurts, J.J., and Hendriks, J.J. (2010). Immunohistochemical detection of synaptic proteins in neuronal tissues using antibodies from the human autoimmune repertoire. *Journal of Neuroscience Research*, 88(4), 777-789. doi: 10.1002/jnr.22258
- Südhof, T. C. (2018). Towards an understanding of synapse formation. *Neuron*, 100(2), 276-293.
- Chen, J., Lin, M., & Foxe, J. J. (2018). Pedunculopontine nucleus and basal ganglia: distant relatives or part of the same family?. *Trends in neurosciences*, 41(5), 247-259
- Basile GA, Bertino S, Bramanti A, Ciurleo R, Anastasi GP, Milardi D, Cacciola A. (2021) Striatal topographical organization: Bridging the gap between molecules, connectivity and behavior. *EUR J Histochem*. 65(s1):3284
- Bamford JJ, Bamford NS. (2019) The Striatum's Role in Executing Rational and Irrational Economic Behaviors. *Neuroscientist*. 25(5):475-490